Journal of Medical Imaging

MedicalImaging.SPIEDigitalLibrary.org

Noise performance of low-dose CT: comparison between an energy integrating detector and a photon counting detector using a whole-body research photon counting CT scanner

Zhicong Yu
Shuai Leng
Steffen Kappler
Katharina Hahn
Zhoubo Li
Ahmed F. Halaweish
Andre Henning
Cynthia H. McCollough

SPIE.

Zhicong Yu, Shuai Leng, Steffen Kappler, Katharina Hahn, Zhoubo Li, Ahmed F. Halaweish, Andre Henning, Cynthia H. McCollough, "Noise performance of low-dose CT: comparison between an energy integrating detector and a photon counting detector using a whole-body research photon counting CT scanner," *J. Med. Imag.* **3**(4), 043503 (2016), doi: 10.1117/1.JMI.3.4.043503.

Noise performance of low-dose CT: comparison between an energy integrating detector and a photon counting detector using a whole-body research photon counting CT scanner

Zhicong Yu,[a] Shuai Leng,[a] Steffen Kappler,[b] Katharina Hahn,[b] Zhoubo Li,[a,c] Ahmed F. Halaweish,[d] Andre Henning,[b] and Cynthia H. McCollough[a,*]
[a]Mayo Clinic, Department of Radiology, 200 First Street S.W. Rochester, Minnesota 55905, United States
[b]Siemens Healthcare, Computed Tomography, Siemensstr. 1, Forchheim 91301, Germany
[c]Mayo Graduate School, 200 First Street S.W. Rochester, Minnesota 55905, United States
[d]Siemens Healthcare, 40 Liberty Boulevard, Malvern, Pennsylvania 19355, United States

Abstract. Photon counting detector (PCD)-based computed tomography (CT) is an emerging imaging technique. Compared to conventional energy integrating detector (EID)-based CT, PCD-CT is able to exclude electronic noise that may severely impair image quality at low photon counts. This work focused on comparing the noise performance at low doses between the PCD and EID subsystems of a whole-body research PCD-CT scanner, both qualitatively and quantitatively. An anthropomorphic thorax phantom was scanned, and images of the shoulder portion were reconstructed. The images were visually and quantitatively compared between the two subsystems in terms of streak artifacts, an indicator of the impact of electronic noise. Furthermore, a torso-shaped water phantom was scanned using a range of tube currents. The product of the noise and the square root of the tube current was calculated, normalized, and compared between the EID and PCD subsystems. Visual assessment of the thorax phantom showed that electronic noise had a noticeably stronger degrading impact in the EID images than in the PCD images. The quantitative results indicated that in low-dose situations, electronic noise had a noticeable impact (up to a 5.8% increase in magnitude relative to quantum noise) on the EID images, but negligible impact on the PCD images. [DOI: 10.1117/1.JMI.3.4.043503]

Keywords: photon counting; computed tomography; low dose; electronic noise.

Paper 16047PRR received Mar. 20, 2016; accepted for publication Nov. 14, 2016; published online Dec. 14, 2016.

1 Introduction

To date, state-of-the-art medical CT scanners use energy integrating detectors (EID) for data acquisition. While such detectors provide numerous benefits in clinical practice, their performance is limited in situations in which the number of incident x-ray photons reaches the level where quantum noise no longer dominates. In such situations, electronic noise, which mainly originates from analog electronic circuits, becomes noticeable or predominant, and thus may severely impair image quality.[1–4]

The clinical impact of electronic noise is most noticeable in large patients and at low doses. In Ref. 4, similar cohorts of obese patients receiving CT colonography (CTC) were evaluated, one group scanned before and the other group scanned after a detector upgrade. All other system parameters remained the same except that the newer detectors had integrated electronics to lower the electronic noise level. Image noise was significantly reduced (by about 10%) in CTC scans using the integrated circuit detector compared with that using a conventional CT detector ($p < 0.001$). This significant noise reduction occurred despite the fact that patient size was larger in the cohort scanned with the integrated circuit detector. Consequently, the authors estimated that a dose reduction of >20% could be achieved if tube current automatic exposure control settings were lowered to match image noise with the conventional CT detectors. Decreased electronic noise, therefore, benefits patient care by either lowering image noise at the same dose, or by lowering the radiation dose (keeping noise level constant).

Photon-counting CT (PCCT) is an emerging imaging technique that may bring new possibilities to clinical practice. It uses a photon counting detector (PCD) that is capable of counting individual incident x-ray photons and resolving their energy information. For a cadmium telluride (CdTe) or cadmium zinc telluride (CZT)-based PCD, pure electronic noise is usually detected as signals with an energy range corresponding to the lower end of a typical CT x-ray spectrum, thus it can be mostly excluded in PCCT by setting a low-energy signal threshold, such as 25 keV.[5] X-ray photons of energies below such a low threshold are unlikely to be from a primary photon transmitted through a patient, and hence unlikely to carry meaningful information. Consequently, excluding low-energy signals does not impair the accuracy of the reconstructed image. Although the number of detected photons is essentially free from the effects of electronic noise, the magnitude of electronic noise is additive to the signal amplitude, and thus the energy associated with a detected photon may be artificially increased to equal the sum of the true signal amplitude and the amplitude of the electronic

*Address all correspondence to: Cynthia H. McCollough, E-mail: mccollough.cynthia@mayo.edu

2329-4302/2016/$25.00 © 2016 SPIE

noise. This may lead to some inaccuracy in the detected x-ray spectrum, but will not create the rapid increase in noise observed with an EID in nonquantum-noise dominated regions.

Recently, our lab has installed a whole-body research PCCT scanner that is based on the second generation dual-source, dual-energy CT scanner (SOMATOM Definition FLASH, Siemens Healthcare, Forchheim, Germany). The research scanner has two x-ray sources that are 95 deg apart, with one coupled to an EID and the other to a PCD, resulting in two independent subsystems, which we refer to as the EID subsystem and the PCD subsystem. Of special note, the EID system uses the integrated circuit design shown by Duan et al.[3] and Liu et al.[4] to have decreased electronic noise compared to more conventional CT detectors types. Thus, the analysis provided here compares PCD to a very low-electronic-noise EID system.

Previously, a systematic evaluation was performed on the PCD subsystem in terms of conventional imaging performance and the impact of the high x-ray flux on PCD image quality.[6] In that study, the PCD subsystem provided CT number accuracy and uniformity that met clinical requirements (±5 HU). The PCD subsystem also delivered energy selective information and presented increased contrast compared to the EID subsystem for high-Z materials. The PCD and EID subsystems had matched in-plane resolution and comparable noise performance, whereas the PCD subsystem had improved spatial resolution in the longitudinal direction. Negligible high-flux effects were noted, even for extreme cases (x-ray flux up to 550 milliampere·seconds (mAs) at 140 kilovolts (kV) for a neonate-sized phantom). In addition, the high-energy bin data demonstrated a reduction of beam hardening artifacts and calcium blooming. As a continuation of that work, we performed a qualitative and quantitative comparison of the noise performance at low-dose levels between the EID and PCD subsystems to determine the relative impact of electronic noise on the EID and PCD subsystems. A preliminary comparison was reported in Ref. 7; this paper presents more thorough and extended results.

2 Materials and Methods

2.1 *Research PCCT System*

A photograph and schematic diagram of the research PCCT scanner are shown in Fig. 1. The two source/detector subsystems allowed direct comparison of EID and PCD results. The EID and PCD subsystems were not operated simultaneously, thus cross scatter between the two subsystems was not a concern. The EID subsystem was equivalent to the A subsystem of the second generation dual-source dual-energy CT system (SOMATOM Definition FLASH, Siemens Healthcare). The

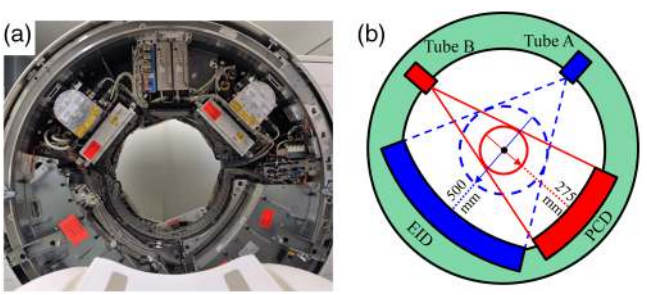

Fig. 1 Illustration of the whole-body research PCCT system. (a) Photograph. (b) Schematic drawing.

EID (Stellar, Siemens Healthcare) was Gd_2O_2S-based and featured fully integrated electronics that have been shown to exhibit very low-electronic noise levels.[3,8] It consisted of 64 rows, with each row containing 736 detector pixels. The width of each EID detector row was 0.6 mm at the iso-center, providing 38.4 mm longitudinal coverage with a field of view (FOV) of diameter 500 mm. The EID was collimated in one dimension: the anti-scatter blades were placed parallel to the longitudinal axis of the scanner for in-plane scatter suppression; see Refs. 6 and 9 for more details.

The PCD used 1.6-mm thick CdTe sensors, which were connected to an ASIC (application-specific integrated circuit). The smallest counting unit on the ASIC, which is called a subpixel, contains two photon counting circuits, allowing for two energy threshold inputs.[6,10] The bias voltage applied between the anode subpixel and the cathode was 1 kV. Although the smallest counting unit was a subpixel, the smallest readout unit at the time of the experiments was a macropixel, which was composed of 4×4 subpixels. The PCD consisted of 32 rows, each of which contained 480 macropixels, providing 16 mm longitudinal coverage and an FOV of diameter 275 mm, both at the iso-center. The PCD was also collimated parallel to the longitudinal axis of the scanner for in-plane scatter suppression. The PCD evaluated here does not use any type of charge-sharing correction, neither in hardware nor in software. Thus, as noted in Ref. 6, some degradation of the spectral separation has been observed.

The PCD subsystem provided two data acquisition modes, namely the macro mode and the chess mode. In the macro mode, all 16 subpixels in one macropixel used the same two energy thresholds, whereas in the chess mode, the 16 subpixels were interlaced into two 8-subpixel groups (like the pattern of a chess board), with one group using one set of energy thresholds, and the other group using a different set of energy thresholds. As was reported in Sec. 2.1 of Ref. 6, the binning process in each macropixel was performed after analog signal processing of the ASIC. Thus, the impact of electronic noise should be identical between the macro mode and chess mode. Hence, this work focused only on the macro mode.

The PCD subsystem provided two beam-shaping (i.e., bow-tie) filters, one configured for head scans and the other for body scans. The 275-mm FOV was large enough for head scans, whereas for body imaging, anatomy was frequently located outside the PCD FOV, and a low-dose data completion scan (DCS) using the EID subsystem was needed.[11] This DCS is used to avoid transverse data truncation artifacts in PCD images. However, it has negligible effect on noise properties.[11]

In order to accurately assess the impact of electronic noise, a special scan mode was provided by the manufacturer that shut off all dose-dependent data filtering methods that would, otherwise, be activated for noise suppression in low-photon-count situations. In the absence of dose-dependent filtration, the in-plane and longitudinal spatial resolution is independent of tube current. This special scan mode was available for both subsystems, but was limited to sequential (axial) scans. Thus, only sequential data were used in this study.

2.2 *Data Acquisition and Analysis*

2.2.1 *Thorax phantom*

The shoulder portion of an anthropomorphic thorax phantom [Fig. 2(a), "Lungman," PH-1, Kyoto Kagaku, Kyoto, Japan] was scanned on both the EID and PCD subsystems for

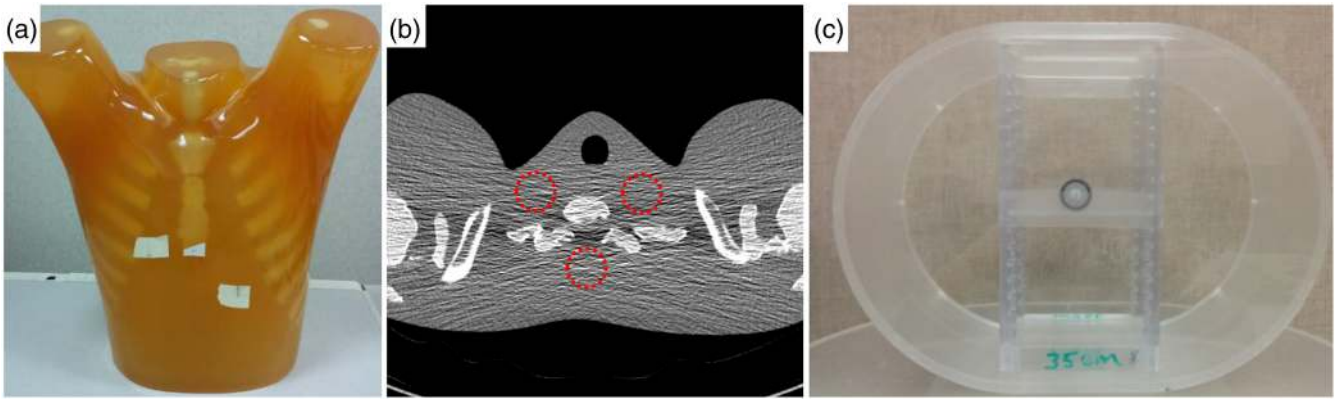

Fig. 2 Phantoms used for low-dose performance assessments. (a) Anthropomorphic thorax phantom ("Lungman," PH-1, Kyoto Kagaku, Kyoto, Japan). The shoulder portion was scanned. (b) Placement of the regions of interest on an axial image of the thorax phantom. (c) Torso-shaped water phantom with lateral width 35 cm. A tungsten wire of diameter 0.05 mm sealed in an air-filled vial was placed near the center of the water phantom for in-plane spatial resolution measurements.

qualitative and quantitative evaluation of streak artifacts. First, a DCS with $CTDI_{vol}$ of 1.01 mGy was acquired for the PCD scan for correction of transverse data truncation.[11] Then, the EID and PCD scans were performed using the special scan mode and a sequential body protocol, 120 kV, and 20, 30, 60, and 120 effective mAs. Among these, 30 mAs provided a dose level equivalent to our lung cancer screening scan protocol. Here, 120 kV was used to reflect current clinical practice and to minimize beam hardening effects, which might obscure the streaks associated with electronic noise. In terms of $CTDI_{vol}$, the dose levels were 1.5 (20 mAs) to 9 mGy (120 mAs) for both the EID and PCD scans. The collimation was 32×0.6 mm on the EID subsystem and 32×0.5 mm on the PCD subsystem. Projection data corresponding to the energy window 25, 120 keV were used for PCD image reconstruction. All images were reconstructed using a quantitative medium smooth kernel (D30) and 1-mm slice thickness. No second-order beam hardening correction was used in either reconstruction. The resultant images were examined visually for the presence of streak artifacts. Regions of interest (ROIs) were placed on the left and right sides of the vertebral body in anterior and posterior positions of the phantom [Fig. 2(b)].

2.2.2 *Quantitative assessment of spatial resolution and noise*

A water phantom containing a tungsten wire was used for noise and in-plane spatial resolution measurements. The water phantom was torso-shaped [Fig. 2(c)], 35-cm wide in the lateral direction, 26-cm high in the anterior–posterior direction, and 13.5-cm long in the longitudinal direction. The tungsten wire was of diameter 0.05 mm inside an air-filled vial, which was placed near the center of the water phantom such that the wire was parallel to the longitudinal direction of the scanner. The water phantom was centered at the iso-center and scanned using the special scan mode on both the EID and PCD subsystems using 80 kV and 16 tube current values, ranging from 40 to 540 mA. For this phantom size, 80 kV was used to ensure that we reached the region in which electronic noise begins to have a meaningful effect on image noise. Based on our experience, we would not expect to see electronic noise effects at higher tube potential settings at this phantom size.

For all PCD scans, a DCS with $CTDI_{vol}$ of 0.81 mGy was acquired for correction of transverse truncation artifacts in the PCD images. Each scan used a body sequential scan protocol with 0.5 s gantry rotation. The collimation was 32×0.6 mm on the EID subsystem and 32×0.5 mm on the PCD subsystem. Projection data corresponding to the energy window [25, 80] keV were used for image reconstruction.

For each EID or PCD scan configuration, two equivalent scans were acquired, and images were reconstructed using the weighted filtered back-projection (WFBP)[12] method with a quantitative medium smooth kernel (D30), 1-mm slice thickness, 1-mm slice increment, and an FOV of 275 mm × 275 mm. Difference images between the two equivalent scans were calculated to remove any structured noise. Noise in the water images was measured for each difference image using a centered circular ROI with diameter 215 mm. The measured noise was averaged across 13 images for each scan configuration.

Generally in CT, variance of the projection data (after the logarithm operation) can be approximated using the following equation:

$$\sigma_{PD}^2 = \frac{1}{E(N)} + \frac{\sigma_e^2}{c^2 E(N)^2}, \tag{1}$$

where σ_{PD} is the noise in the projection data, σ_e is the electronic noise, $E(N)$ is the expected quanta, and c is a system specific scalar.[13] To propagate the variance in the projection domain into the image domain, all intermediate steps in the reconstruction pipeline must be considered, like interpolations or filtering with the convolution kernel, which introduce correlations into the noisy data. This makes analytical description of noise variance in the reconstructed data more difficult. A detailed discussion of the propagation of noise through the WFBP reconstruction[12] is given in Chapter 7 of Ref. 13. Here, a simplified description of noise variance in the reconstructed image is assumed, with all correlations neglected. In this scenario, and using tube current I as a surrogate for the expected quanta (kV was held constant), noise in the image σ can be expressed as

$$\sigma \propto \sqrt{\frac{1}{I} * \left(1 + \frac{\sigma_e^2}{c^2 I}\right)}. \tag{2}$$

When the tube current is high, the electronic noise term becomes small and $\sigma \propto 1/\sqrt{I}$. Thus, for a tube current I and average noise $\sigma(I)$, the product P of the averaged noise and the square root of the tube current can be calculated [Eq. (3)], and further normalized by dividing by the product corresponding to the highest tube current 540 mA [Eq. (4)]

$$P(I) = \sigma(I) \times \sqrt{I}, \tag{3}$$

$$\bar{P}(I) = P(I)/P\,(I = 540\ \text{mAs}). \tag{4}$$

The normalized product denoted as $\bar{P}$ was calculated and plotted against tube current I for both subsystems. In the absence of electronic noise, when only quantum noise is present, the normalized product should be equal to unity across all tube currents. This assumes that all other factors affecting noise and spatial resolution were kept constant. This assumption was valid, as all dose-dependent filtration was disabled in our study. However, to experimentally validate this assumption, the in-plane spatial resolution was assessed in terms of modulation transfer function (MTF) at two substantially different tube currents, 80 and 420 mA, using the tungsten wire phantom. First, images of the tungsten wire were reconstructed using the WFBP method with a quantitative medium smooth kernel (D30), 2-mm slice thickness, and an FOV of 50 mm × 50 mm. In each image, the pixel with the maximum CT number was identified, and the background was subtracted. A 2-D point spread function (PSF) centered at this pixel was then generated, which was radially averaged to generate a 1-D line profile. Finally, the line profile was Fourier transformed and normalized to its DC component to generate the MTF curve.[6]

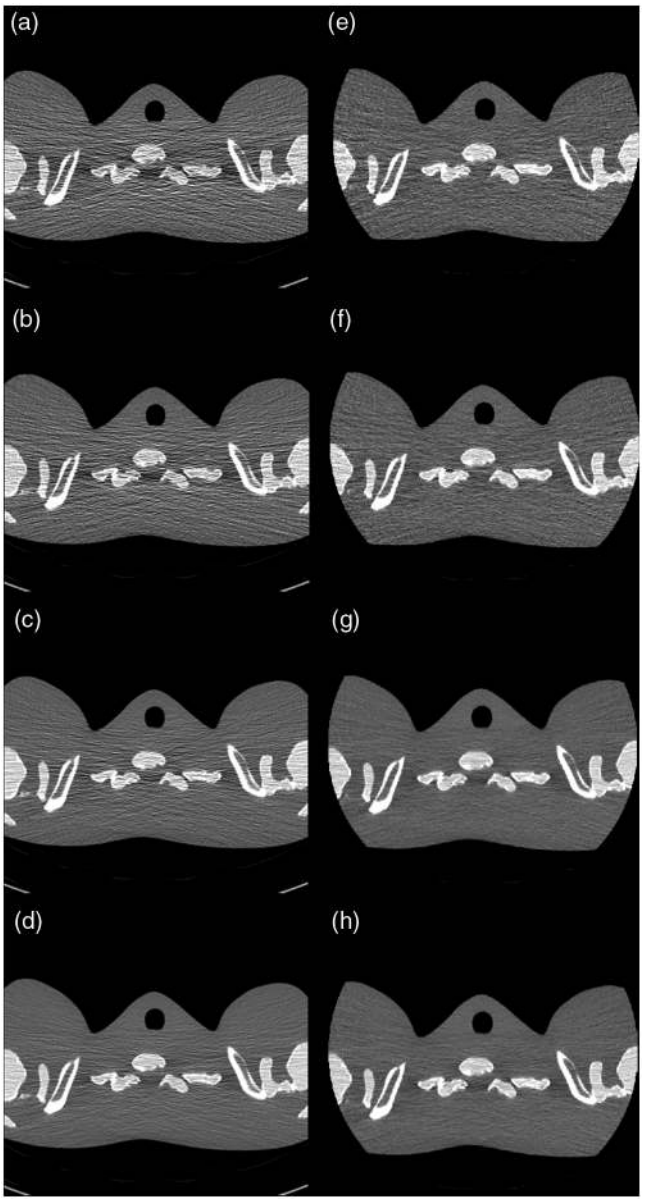

Fig. 3 Images of the shoulder phantom at various dose levels. (a)–(d) Images from the EID subsystem at 20, 30, 60, and 120 mAs, respectively. (e)–(h) Images from the PCD subsystem at 20, 30, 60, and 120 mAs, respectively. The PCD images had noticeably less horizontal streak artifacts and an overall more uniform appearance than the EID image. Beam hardening artifacts (dark banding) were present in both images. Display window: $W/L = 900/40$ HU.

3 Results

The reconstructed images of the shoulder of the thorax phantom are shown in Fig. 3. Compared to the EID image, which was formed using a very low electronic noise detector (Stellar detector, Siemens Healthcare),[8] the PCD image presented noticeably less horizontal streak artifact and an overall more uniform appearance. When the mAs was reduced from 120 to 20, the amount of streak artifacts increased more in the EID images than in the PCD images, indicating that electronic noise was better controlled in the PCD compared to the EID. Beam-hardening artifacts (dark banding) were present in both the EID and PCD images. Standard deviation in the three ROIs and their mean value are shown in Table 1.

The MTF curves are shown in Fig. 4 for both the EID and PCD subsystems. For each subsystem, the MTF curves were almost identical between 80 and 420 mA, indicating that the in-plane spatial resolution did not change across different tube currents, which confirmed that dose-dependent filtration indeed was disabled.

The normalized product $\bar{P}$ is plotted against tube current in Fig. 5. For the EID subsystem, the normalized product was equal to unity for tube currents higher than 240 mA. When the tube current decreased from 240 to 60 mA, the normalized

Table 1 Standard deviation of CT numbers (in HU), and their mean values, are shown for the EID and PCD at 20, 30, 60, and 120 mAs.

	mAs	Center	Left	Right	Mean
EID	20	166	153	142	154
	30	134	137	132	134
	60	80	96	100	92
	120	54	64	65	61
PCD	20	77	76	73	75
	30	72	57	68	66
	60	50	51	44	48
	120	36	35	36	36

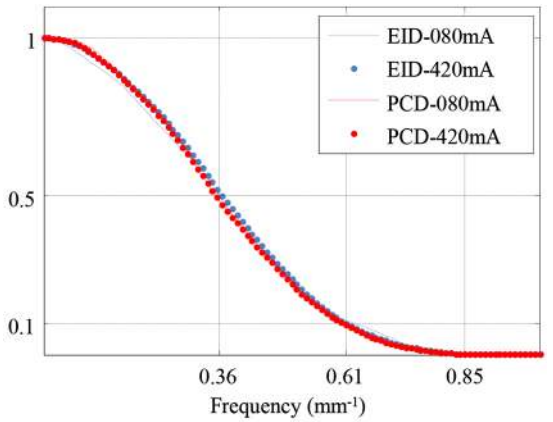

Fig. 4 Measurement of in-plane spatial resolution. For each subsystem, there was no noticeable difference in the measured MTF curves between 80 and 420 mA, indicating consistent in-plane spatial resolution across different tube currents.

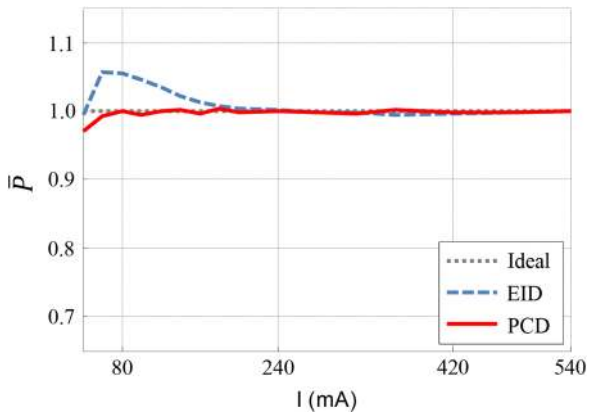

Fig. 5 Normalized product of noise and square root of tube current. The normalized product for the EID subsystem was >1 at low tube currents, which is evidence of electronic noise. The normalized product for the PCD subsystem was 1 for tube currents between 80 and 540 mA.

product gradually increased. At around 60 mA, the normalized product reached a maximum (1.058). It then started to decrease as tube current decreased further. For the EID subsystem, the deviation from 1 of the normalized product between 60 and 240 mA was caused by the no longer negligible impact of electronic noise in low-dose signals. The turning point at 60 mA was due to data clipping at extremely low signal values. For low photon fluence, measurements of the photon quanta can be nonpositive due to the noise envelope that is centered essentially about zero signal. Because the logarithm is defined for positive signal values only, "clipping" of the noisy data, by setting all negative values to a minimum positive value, is required. This shifts the measured data to a higher number, making the signal appear higher than it is and leading to lower than expected noise levels in the image domain. The signal amplitude where clipping was performed was comparable for both subsystems.

For the PCD subsystem, the normalized product equaled unity between 80 and 540 mA, which indicated that the PCD images were free of electronic noise effects. A turning point at 80 mA was observed due to the aforementioned data clipping prior to the logarithm operation.

For both subsystems, the measurement precision of the normalized product $\bar{P}$ was dominated by photon statistics and the accuracy of the x-ray tube intensity output. Using error propagation of the variability of image noise (by measuring its standard deviation in 13 difference images) and assuming the x-ray tube intensity accuracy to be better than 1.5% (flatly distributed), we obtained a precision of 0.6% (standard deviation) for the normalized product.

4 Discussion and Summary

The special data acquisition mode used excluded all data filtering processes that were designed to suppress noise in low-photon-count scenarios. Thus, spatial resolution is expected to be independent of tube current. In this work, we validated this assumption for only the in-plane spatial resolution, as longitudinal spatial resolution measurements are difficult to obtain in sequential acquisition modes, in part due to limitations in the sequential incrementation accuracy of the patient table. However, in the system used, the dose-dependent longitudinal data filtration is strictly coupled to the in-plane filtration. Thus, finding no evidence of dose-dependent filtration in the image plane, we were confident that such filtration was also disabled in the longitudinal direction. The longitudinal spatial resolution was, however, different for the EID subsystem versus the PCD subsystem due to the difference in the detector pitch (0.6 mm versus 0.5 mm, at iso-center, respectively). However, provided that the spatial resolution was constant across dose within a given subsystem (as discussed above), matching of the spatial resolution between the two subsystems is not necessary for the comparison of $\bar{P}$ as $\bar{P}$ is a relative measurement, which normalized the noise at any one tube current to the noise at the maximum tube current.

Even though the EID used in this study is cutting-edge in terms of having a very low electronic noise level,[3] the presented work demonstrated no evidence of electronic noise for the PCD. The ability to threshold-out electronic noise is an intrinsic advantage of PCD technology.

One limitation of this work is the lack of a theoretical derivation of the expected behavior of $\bar{P}$ as a function of electronic noise for the specific reconstruction algorithm used in this study WFBP.[12] While it is clear that the addition of electronic noise will increase noise relative to what would be expected when only quantum noise is present, the absolute percent increase is not predicted in this work for comparison to the measured values. This is due to the complexity of propagating the noise in the projection domain through the image reconstruction pipeline when the rebinned projection data are correlated, which would require that a number of assumptions be made[13] and that proprietary information be shared. We thus elected to perform an empirical analysis of the normalized impact of electronic noise as dose is reduced. Furthermore, as all dose-dependent filtration algorithms were disabled to evaluate the detector characteristics only, absolute changes in noise as a function of dose would not likely correspond to what would be observed on a commercial system.

Another limitation of this work is that a thorough and detailed comparison of detection efficiency between the EID and PCD subsystems was not provided, resulting in difficulties in directly comparing electronic-noise impact between the two subsystems. However, according to our previous work,[6] noise performance in the high-dose regime was almost identical between EID images and threshold-low PCD images in the macro mode. Furthermore, the qualitative assessment of the

shoulder phantom also indicated that electronic noise had a more noticeable impact on the EID images than on the PCD images. Note that, for the anthropomorphic shoulder phantom, streak artifacts dominated in the horizontal direction in Fig. 3. Consequently, the standard deviation measurements reported in Table 1 included both noise and substantial artifacts. These standard deviation measurements are used to demonstrate the extent of the streak artifacts, and, thus, are deemed inappropriate for noise comparison.

In summary, we have presented a comparison of the noise performance at low-dose levels between the EID and PCD subsystems of a whole-body research PCCT scanner. The qualitative results showed less streak artifacts and a more uniform noise texture for the PCD images compared to the EID images. When mAs was reduced, electronic noise had a noticeably stronger degrading impact in the EID images than in the PCD images. The quantitative results indicated that in low-dose situations, the impact of electronic noise was noticeable (up to a 5.8% increase relative to quantum noise alone) on the EID images, but negligible on the PCD images.

Disclosures

Dr. McCollough receives grant funding from Siemens Healthcare. Drs. Kappler, Hahn, Henning, and Halaweish are employees of Siemens Healthcare. No other authors have a potential conflict of interest.

Acknowledgments

The project described was supported by Grant Nos. R01 EB016966 and C06 RR018898 from the National Institutes of Health in collaboration with Siemens Healthcare. The content is solely the responsibility of the authors and does not necessarily represent the official views of the National Institutes of Health. The equipment and concepts described in this work are based on a research device and are not commercially available. The authors would like to thank Dr. Thomas Allmendinger for his support in reconstructing the PCD image of the shoulder phantom. The authors would also like to thank Kristina Nunez for her assistance with paper preparation. The authors also would like to thank the editor and reviewers for their constructive comments and suggestions.

References

1. B. R. Whiting et al., "Properties of preprocessed sinogram data in x-ray computed tomography," *Med. Phys.* **33**(9), 3290–3303 (2006).
2. P. Massoumzadeh et al., "Validation of CT dose-reduction simulation," *Med. Phys.* **36**(1), 174–189 (2009).
3. X. Duan et al., "Electronic noise in CT detectors: impact on image noise and artifacts," *Am. J. Roentgenol.* **201**(4), W626–W632 (2013).
4. Y. Liu et al., "Reducing image noise in computed tomography (CT) colonography: effect of an integrated circuit CT detector," *J. Comput. Assist Tomogr.* **38**(3), 398–403 (2014).
5. J. S. Iwanczyk et al., "Photon counting energy dispersive detector arrays for x-ray imaging," *IEEE Trans. Nucl. Sci.* **56** (3), 535–542 (2009).
6. Z. Yu et al., "Evaluation of conventional imaging performance in a research whole-body CT system with a photon-counting detector array," *Phys. Med. Biol.* **61**(4), 1572–1595 (2016).
7. Z. Yu et al., "Low-dose performance of a whole-body research photon-counting CT scanner," *Proc. SPIE* **9783**, 97835Q (2016).
8. S. Ulzheimer and J. Freund, *The Stellar Detector*, Siemens Healthcare, Forchheim, Germany (2012).
9. R. Gutjahr et al., "Human imaging with photon counting based computed tomography at clinical dose levels: contrast-to-noise ratio and cadaver studies," *Invest Radiol.* **51**, 421–429 (2016).
10. S. Kappler et al., "A research prototype system for quantum-counting clinical CT," *Proc. SPIE* **7622**, 76221Z (2010).
11. Z. Yu et al., "How low can we go in radiation dose for the data-completion scan on a research whole-body photon-counting CT system," *J. Comput. Assist. Tomogr.* **40**, 663–670 (2016).
12. K. Stierstorfer et al., "Weighted FBP—a simple approximate 3D FBP algorithm for multislice spiral CT with good dose usage for arbitrary pitch," *Phys. Med. Biol.* **49**(11), 2209–2218 (2004).
13. A. Borsdorf, "Adaptive filtering for noise reduction in x-ray computed tomography," PhD Thesis, University of Erlangen (2009), http://www5.informatik.uni-erlangen.de/Forschung/Publikationen/2009/Borsdorf09-AFF.pdf (August 11 2016).

Zhicong Yu was a research fellow at Mayo Clinic, Rochester, MN, USA. He received his PhD from University of Erlangen-Nuremberg, Germany, in 2013. His research interests include CT/C-arm physics and imaging, with emphasis on photon-counting CT and advanced image reconstruction techniques.

Shuai Leng received a BS degree in engineering physics in 2001, an MS degree in engineering physics in 2003, from Tsinghua University, and a PhD in medical physics in 2008 from the University of Wisconsin, Madison. He is an associate professor of medical physics at the Mayo Clinic in Rochester, MN. He has authored over 100 peer-reviewed articles. His research interest is technical development and clinical application of x-ray and CT imaging.

Cynthia H. McCollough received a BS degree in physics from Hope College in 1985, a MS degree in medical physics from the University of Wisconsin, Madison, in 1986, and a PhD in medical physics from the University of Wisconsin, Madison, in 1991. She is a professor of medical physics and biomedical engineering at the Mayo Clinic in Rochester, MN, where she directs the multidisciplinary CT Clinical Innovation Center.

Biographies for the other authors are not available.